JTTEE5 15:802-810
DOI: 10.1361/105996306X146721
1059-9630/$19.00 © ASM International

Peer Reviewed

Heat Treatment Effects on the Tribological Performance of HVOF Sprayed Co-Mo-Cr-Si Coatings

G. Bolelli and L. Lusvarghi

(Submitted February 28, 2006; in revised form April 13, 2006)

The tribological behavior of high-velocity oxyfuel sprayed Co-28%Mo-17%Cr-3%Si coatings, both as-sprayed and after heat treatments at 200, 400, and 600 °C for 1 h, has been studied. The as-sprayed coating contains oxide stringers and is mostly amorphous. It has low hardness (~6.7 GPa) and toughness and undergoes adhesive wear against 100Cr6 steel. The friction coefficient increases up to ~0.9, so the flash temperature reaches a critical oxidation value; then, friction decreases and increases again. This phenomenon occurs periodically. Much adhesive wear occurs in the first stage. Abrasive wear prevails against alumina pin: the coating wear rate is lower because it possesses good plasticity. Thermal effects still occur. The 600 °C treatment causes formation of submicrometric crystals. Hardness increases (~8.8 GPa), adhesive wear is prevented, the friction coefficient has no peaks. Against the alumina pin, wear rates remain similar to the as-sprayed case. Nevertheless, the friction coefficient has no peaks and its final value is lowered (from 0.84 to 0.75).

Keywords cobalt alloy, high-velocity oxyfuel spraying, pin-on-disk test, posttreatment, sliding wear

1. Introduction

High-velocity oxyfuel (HVOF) spraying is largely used for manufacturing tribological coatings and as hard chrome plating alternative. A wide range of coating materials are available: metals, cermets (Ref 1), and sometimes even ceramics (Ref 2). The tribological behavior of WC- and Cr_xC_y-based HVOF sprayed cermet coatings and their potential use as hard chrome replacement have already been the object of much research (Ref 3-8). Since they are hard and tough, they often display the best performance against wear. Nonetheless, other coating materials could be preferable in certain situations. Cermet powders are often more expensive than metallic ones; cermets are difficult to grind and polish; use of metallic alloys with good high-temperature strength could be more advisable in hot environments. Thus, also HVOF sprayed metals must be considered for tribological applications.

Several studies exist on self-fluxing NiCrBSi alloys (Ref 9-14). Their corrosion resistance makes them fit for tribocorrosion conditions, but their hardness is never particularly high, so their sliding wear performance cannot challenge cermets (Ref 3). The potentialities of Co-28%Mo-17%Cr-3%Si alloy, declared by manufacturers to possess good sliding wear resistance from room temperature up to 800 °C, are of interest. Very few literature studies on them exist (Ref 6, 15-21). They are precipitation-strengthening alloys (Ref 15), but become mostly amorphous (metallic glasses) when thermally sprayed (Ref 15, 17). Metallic glasses are also very promising materials (Ref 22), but these special alloys are designed to fully benefit from the glassy structure advantages: the present alloy, instead, should form hard intermetallics; an amorphous microstructure is not a favorable condition. The room-temperature sliding performance of the coating may be improved if a proper heat treatment could produce at least partial crystallization of the thermally sprayed coating, thus exploiting the precipitation-hardening mechanisms.

The aim of this research is to verify whether simple, economic heat treatments can actually improve the dry sliding performance of HVOF sprayed Co-28%Mo-17%Cr-3%Si coating at room temperature, acquiring satisfactory tribological properties, similar to those of electrolytic hard chrome platings.

2. Materials and Characterization

The Praxair-Tafa JP5000 HVOF torch owned by Centro Sviluppo Materiali S.p.A. (Roma, Italy) was used to spray Co-28%Mo-17%Cr-3%Si powders (Diamalloy 3001NS, Sulzer Metco, Winterthur, Switzerland). Spray parameters are as follows: 203.2 mm gun barrel, 944 sLpm in O_2 flux, 0.379 L/min kerosene flux, 4.7 L/min carrier gas (N_2) flux, 7.1 bar combustion pressure, and 350 m spraying distance. AISI 1040 steel plates (100 by 100 by 5) mm^3 have been used as substrates. Grit blasting with 500 mesh alumina particles was performed immediately before coating deposition.

HVOF sprayed coatings were heat treated at 200, 400, and

This article was originally published in *Building on 100 Years of Success, Proceedings of the 2006 International Thermal Spray Conference* (Seattle, WA), May 15-18, 2006, B.R. Marple, M.M. Hyland, Y.-Ch. Lau, R.S. Lima, and J. Voyer, Ed., ASM International, Materials Park, OH, 2006.

G. Bolelli and **L. Lusvarghi,** Dipartimento di Ingegneria dei Materiali e dell'Ambiente, University of Modena and Reggio Emilia, Via Vignolese 905, 41100 Modena, Italy. Contact e-mail: bolelli.giovanni@unimore.it; lucalusv@unimore.it.

600 °C for 1 h in an electric kiln in air (10 °C/min heating rate, sample cooling inside the kiln); both as-deposited and treated coatings were studied. Polished cross sections (mounted in resin) were observed by scanning electron microscopy (SEM) (ESEM Quanta-200, FEI, Eindhoven, The Netherlands) and used for depth-sensing microindentation (Depth-Sensing Vickers microindenter, CSM Instruments, Peseux, Switzerland). A 1 N (~100 g) load was used for Vickers microhardness evaluation (optical indentation diagonal measurement), 5 N for elastic modulus (Oliver-Pharr procedure, Ref 23, 4 N/min loading and unloading rates, 15 s loading time, Poisson's ratio assumed to be 0.30), 10 N for indentation fracture toughness (Evans and Charles formula, Ref 24, microcracks measured by SEM). Powders and polished surfaces were analyzed by x-ray diffractometry (X'pert Pro, PANalytical, The Netherlands). Simultaneous thermogravimetry-differential thermal analysis (TG-DTA) in air (10 °C/min heating rate up to 1400 °C) was performed on the powder (STA 429 CD/7/G DTA-TG analyzer, Netzsch, Selb, Germany). Rotating unidirectional dry sliding tribological tests were performed on polished samples ($R_a \approx 0.1$ μm) with a pin-on-disk tribometer (CSM Instruments) against 100Cr6 balls (6 mm diameter, manufacturer's nominal hardness HV = 7 GPa) and sintered alumina balls (6 mm diameter, manufacturer's nominal hardness HV = 19 GPa). Test conditions were 5 N normal load, 0.20 m/s sliding speed, and 250 m total sliding distance. The radius between the pin position and the sample revolution axis was fixed at 5 mm. The friction coefficient was on-line monitored during the test, the diameter of the ball wear scar was measured by optical microscopy to assess its wear rate, and sample wear rate was calculated by measuring the average cross-sectional area of the wear track by optical profilometry (ConScan profilometer, CSM Instruments), computing the resulting wear volume.

3. Results and Discussion

3.1 Microstructural and Micromechanical Characterization

Showing consistency with former data (Ref 15, 17), as-sprayed coatings display low porosity but some interlamellar oxidation (Fig. 1). TG-DTA performed on the spray powder highlights marked exothermal peaks (812, 1030, and 1130 °C), with an overall ~30% weight gain, probably due to oxidation of the powder. They are clearly the reason for the high degree of in-flight particle oxidation, which is unusual for HVOF sprayed coatings manufactured with kerosene-fueled torches. In a homogeneous matrix, few crystalline areas, with bright crystals richer in Mo and a darker surrounding area richer in Cr, emerge (Fig. 2); x-ray diffraction (XRD) suggests the matrix is mostly amorphous while bright crystals are Co_7Mo_6, Co_3Mo, and Co_3Mo_2Si (Fig. 3). These areas are often located in the core of lamellae, so they might be unmolten regions preserving the original powder microstructure, but there is no clear evidence. Since the spray powder is crystalline and possesses sharp diffraction peaks (indicating quite large crystals with low defect density, Fig. 3), powder particles were probably almost completely molten during spraying, and the extremely high cooling rate of splats upon impact impeded subsequent crystal nucleation and growth.

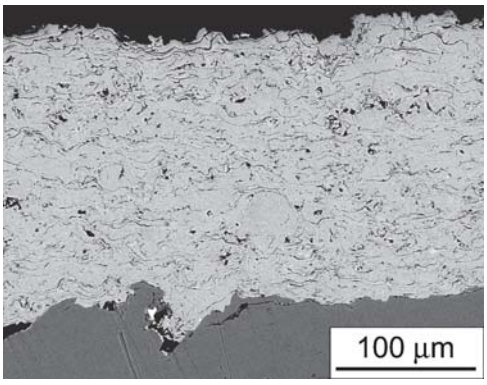

Fig. 1 Cross-sectional SEM micrograph of as-sprayed Co-Mo-Cr-Si coating

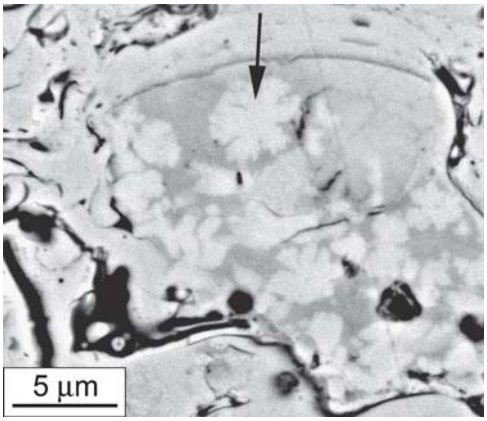

Fig. 2 Detail of crystalline region in as-sprayed Co-Mo-Cr-Si coating. Arrow indicates Mo-rich crystals.

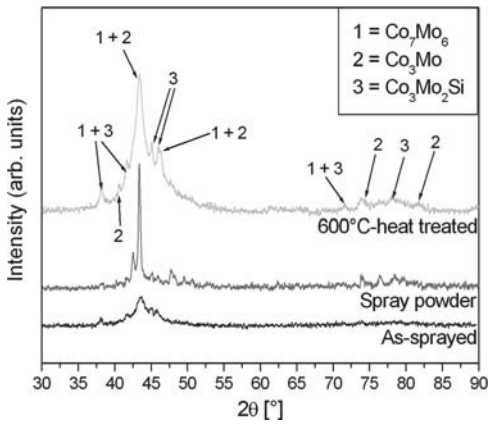

Fig. 3 XRD patterns of as-deposited and 600 °C heat treated coatings and of spray powder

However, other metallic alloys sprayed by HVOF technique (such as Ni-base bond coats or Ni-Cr-B-Si alloys) develop a higher degree of crystallinity, which would suggest that nucleation and/or growth kinetics of Co-Mo-Cr-Si alloys are quite slow. This hypothesis would be corroborated by the fact that the

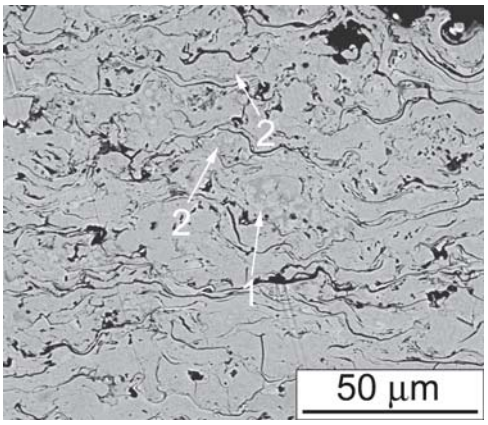

Fig. 4 SEM micrograph of 600 °C heat treated coating. Areas with larger (1) and smaller (2) crystals are indicated.

Co-base matrix in HVOF sprayed cermets has frequently been found to be amorphous as well (Ref 17, 25). However, this point requires further research.

After heat treatments at 200 and 400 °C, no major changes occur. After the heat treatment at 600 °C, more crystalline regions appear: besides the already-described areas containing micrometric crystals (Fig. 4, labeled as 1), regions with smaller, submicrometric crystals now exist (Fig. 4, labeled as 2). The small crystal size in this latter kind of crystalline regions might indicate that, at 600 °C, crystals growth rate is low. Since newly formed crystals are small, XRD patterns do not show major changes, but more intense and better-defined peaks appear (Fig. 3).

Due to such microstructural changes, micromechanical differences exist between as-sprayed and 600 °C heat treated coatings: hardness and elastic modulus significantly increase (Fig. 5a and b). This indicates that the intrinsic properties of the material have been modified. No increase has been noticed for the coatings heat treated at 200 and 400 °C. The 200 °C heat treated coating even seems to have been slightly weakened (even though the differences between average values are in the range of the standard deviation). Maybe, some limited solid-solution strengthening effect exists in the as-sprayed alloy due to lattice distortions by supersaturated solute elements (Mo, Si). It may be argued that the 200 °C heat treatment relieves these lattice strains and weakens the material. Fracture toughness also slightly decreases after the 200 °C heat treatment and increases after the 600 °C treatment, but this latter increase is not as large as the one noted for hardness and elastic modulus (Fig. 5c). Splat boundaries, the weakest link in most thermally sprayed coatings, are, in all tested coatings, the preferential crack propagation path. In all thermally sprayed coatings, limited interlamellar cohesion is a reason for low toughness, but, in this specific case, brittle intersplat oxide inclusions significantly contribute to interlamellar cracking. The 600 °C thermal treatment toughens the metallic alloy thanks to the submicrometric crystal formation, but cannot remove splat boundary oxide inclusions, so that toughness improvement, even though perceivable, is not very large. Moreover, inclusions hinder diffusion along splat boundaries, which would have improved intersplat cohesion and hence toughness.

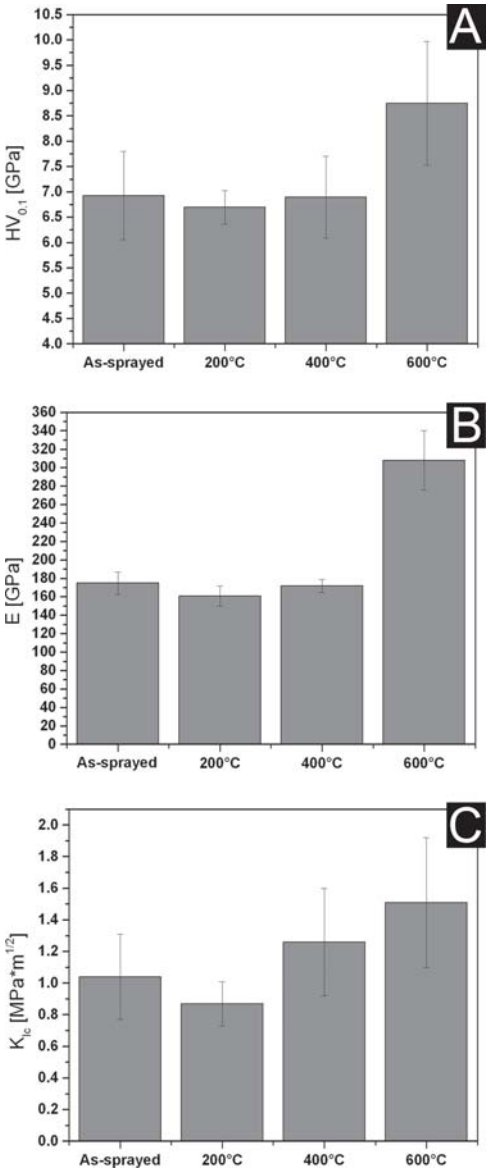

Fig. 5 (a) Vickers microhardness $HV_{0.1}$, (b) elastic modulus from instrumented indentation, and (c) indentation fracture toughness K_{Ic} [MPa · m$^{1/2}$] for as-sprayed and heat treated coatings

3.2 Tribological Characterization

As-deposited coating and coatings heat treated at 200 and 600 °C have been characterized; the one heat treated at 400 °C, which did not differ from the one heat treated at 200 °C, has not been further examined.

The qualitative behavior of the 200 °C heat treated coating, in terms of friction coefficient evolution and wear scar morphology, does not differ significantly from the behavior of the as-sprayed coating, but, quantitatively, the wear rate is higher both against alumina and against 100Cr6 (Table 1). The wear rate for both coatings is higher against 100Cr6 than against alumina.

In both cases, the friction coefficient follows a peculiar evolution (Fig. 6): in the first stage of the test, the friction coefficient soon reaches a very high value. After a certain sliding distance,

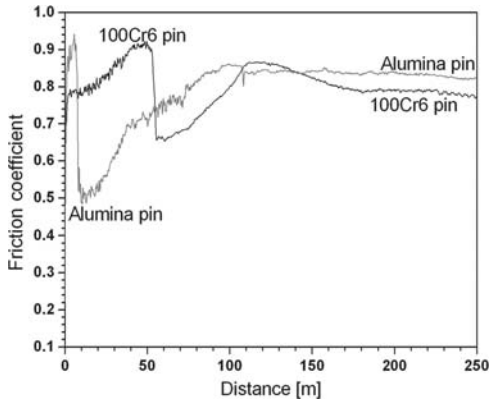

Fig. 6 Friction coefficient for the as-sprayed coating tested against 100Cr6 steel and sintered alumina pins over a 250 m sliding distance

Table 1 Pin-on-disk test results

	As sprayed	200 °C	600 °C
Sample wear rate, $\times 10^{-5}$ mm^3/(Nm)			
A	1.96	8.28	2.11
S	19.0	34.2	Negligible
Pin wear rate, $\times 10^{-6}$ mm^3/(Nm)			
A	0.796	6.86	0.521
S	18.4	8.40	0.216
Friction coefficient			
A	0.84 ± 0.01	0.82 ± 0.01	0.73 ± 0.03
S	0.79 ± 0.01	0.80 ± 0.02	0.79 ± 0.02
Peak friction coefficient			
A	0.90 ± 0.05	0.86 ± 0.05	No friction peak
S	0.91 ± 0.02	0.90 ± 0.02	No friction peak

A, alumina pin as counterbody; S, 100Cr6 steel pin as counterbody

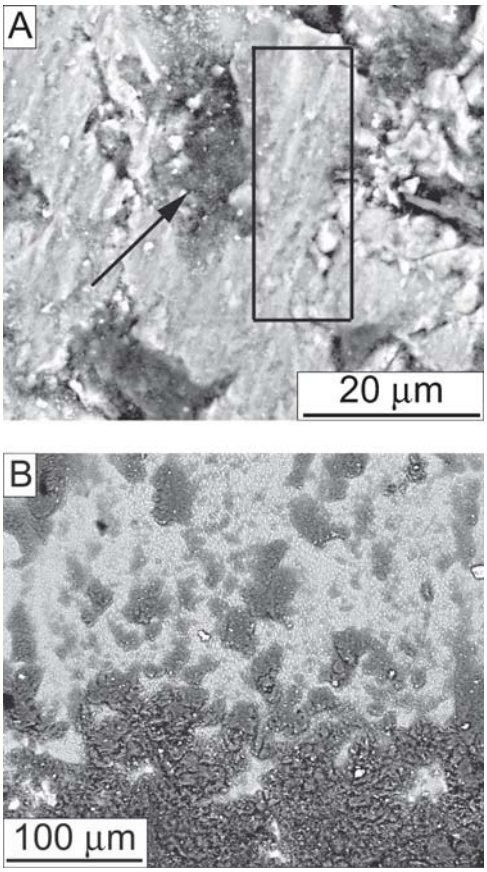

Fig. 7 SEM micrograph of wear scar on (a) as-sprayed coating and (b) 100Cr6 steel pin. The rectangle indicates evidence of adhesive wear, the arrow indicates dark oxides.

shorter in the case of alumina counterpart than for steel counterpart, a great amount of oxide debris is formed, and simultaneously the friction coefficient markedly decreases to a minimum value, retained for a very short distance (a few meters). Then, friction coefficient increases again. In the case of the alumina pin, friction then seems to attain a stable value. In the case of the steel pin, it again shows a peak and a decrease before reaching a seemingly stable value (this stable value is indicated in Table 1). A tentative explanation for this phenomenon is discussed later in this paper.

Significant adhesive wear probably occurs for as-sprayed and 200 °C heat treated coatings tested against 100Cr6 steel; indeed, evidence of this wear mechanism can be found, for instance, on the as-sprayed coating wear scar (Fig. 7a, area in rectangle). As described in Ref 26 to 28, adhesive wear occurs because surface asperities of the two bodies plasticize when coming into contact, since the actual contact pressure they have to bear is significantly higher than the nominal one; the real contact area, in fact, is definitely smaller than the nominal one due to the rough, nonideal profile of any real surface. Plastic deformation of contacting asperities results in the formation of junctions; that is, the asperities are locally "welded" together. To keep relative motion between the two bodies, junctions must be broken up: the fracture may occur either at the exact junction point, or inside one of the two bodies. In the latter case, the fracture generally occurs inside the surface having lower hardness (since hardness is connected to local yield strength) and results in direct wear loss on this surface, with material transfer to the counterbody. In the former case, no direct wear loss occurs, but asperities undergoing repeated plastic deformation are subject to a very severe fatigue process, which soon causes the nucleation and growth of a surface crack, resulting in the detachment of very small, plateletlike wear debris. This debris can remain in the contact area, be expelled, or stick to one of the surfaces, thus contributing to the formation of the transfer film. In this case, evidence of small asperities being torn away from the coating surface and transferred to the pin surface is clearly present in Fig. 7a (see area in the box) and 7b (transferred material on the pin appears as small protrusions on its surface). Energy dispersive spectroscopy (EDS) analysis confirms that Co, Mo, Cr, and Si are the main constituents of this transferred material. Some pin wear loss also occurs; however, steel pin wear rates are one order of magnitude lower than the coating ones, and no significant material transfer occurs from pin to coating. Adhesive wear obviously causes much friction, since a high tangential force must be applied to break junctions apart; this can be the reason for the high friction coefficient in the first stage of the test. It must also be noticed that high friction results in high flash temperatures in the contacting asperities: much heat is generated on the small real contact area due to friction (Ref 26-29). Thus, the

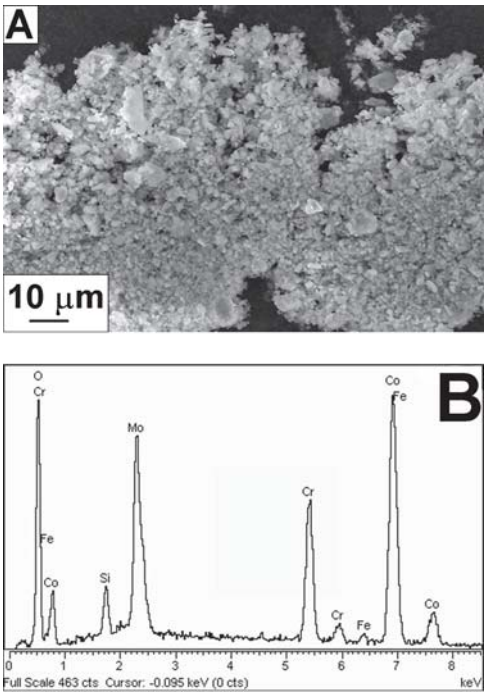

Fig. 8 SEM micrograph of oxide debris collected after testing the as-sprayed coating against 100Cr6 steel pin (a) and (b) EDS microanalysis

local hardness of contacting asperities decreases and adhesion progressively increases, further favoring high friction. Besides, as the film of transferred material on the pin surface grows, a larger part of the contact involves surfaces with the same chemical composition: higher chemical affinity increases friction.

After the friction peak has been attained, a fast friction decrease with the generation of much oxide debris is found. EDS analysis (Fig. 8b) indicates that both the loose debris particles (Fig. 8a) and the oxides remaining adherent to the surfaces contain coating constituents (Co, Cr, Mo, Si). Their formation is due to a very rapid oxidation of the coating material: TG-DTA analysis has shown that significant oxidation of the coating material starts only at temperatures above 800 °C. This might seem strange because, at such high temperatures, the steel pin, consisting of a martensitic steel, should be largely softened; however, there is no evidence of such softening. This apparent contradiction can be easily understood by considering that, as mentioned previously, adhesive wear has generated a film of transferred material on the pin surface. Besides, some very small plateletlike debris from the coating might also be present due to adhesive wear. Thus, a coating-transferred film contact or a three-body contact involving fine debris particles is now taking place. The flash temperature attained by asperities during the contact time (few microseconds) can be much higher than the equilibrium bulk temperature of the body: much heat is generated in a very small volume when plastic junctions are broken. Thus, asperities on the coating and on the transfer film may have reached the critical oxidation temperature even though the bulk temperature is much lower, thus causing oxidation. Since the transfer film also consists of coating material, oxides contain almost no iron, and the steel pin does not soften.

This also means that this sudden change is related to a wear

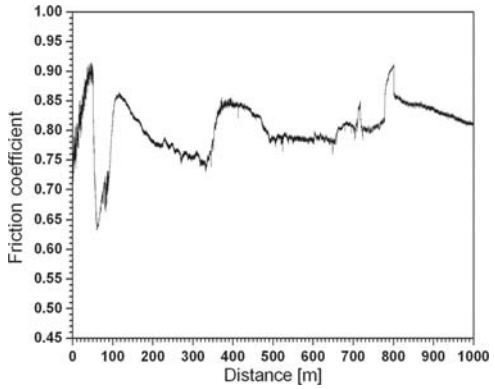

Fig. 9 Friction coefficient for the as-sprayed coating tested against 100Cr6 steel pin over a 1000 m sliding distance

mechanism transition: from adhesive wear to tribo-oxidative wear. The loose oxide particles found on the coating surface (Fig. 8a) are actually aggregates of very small particles; their morphology is quite typical of tribo-oxidative wear mechanisms, as indicated in (Ref 28). Oxides markedly reduce adhesion between the contacting surfaces, both because they reduce chemical affinity between contacting surfaces and because Co and Mo oxides are known to possess self-lubricating properties. If these oxides were perfectly adherent, friction would remain low; unfortunately, many are detached as loose wear debris and the contacting surfaces are not covered by continuous oxide films. Thus, some metallic areas are still exposed and adhesive wear once again occurs; thus, the cycle starts again with a friction increase. After approximately 180 m, friction seems to attain a stable value; however, to verify the behavior of the system over a larger sliding distance, a pin-on-disk test against 100Cr6 steel has been performed with a 1000 m sliding distance (Fig. 9); although some short stable stages are found, the friction coefficient has periodic peaks, up to the critical oxidation value, and subsequently decreases. The sample wear scar after a 1000 m sliding distance (Fig. 10a) shows some very large oxide inclusions, which mainly consist of small oxidized particles stuck together (Fig. 10b), and uncovered metallic zones, which are responsible for the continuous onset of adhesive wear. It is likely that the oxide formation helps controlling friction (reduced chemical compatibility of the surfaces and self-lubricating properties of the oxides), but the poor oxide adhesion to the coating surface still allows adhesive wear, so that peaks can still occur when flash temperature increases. Subsequent oscillations, however, are smaller than the first one.

It is known that adhesive wear causes one order of magnitude higher wear rates than tribo-oxidative wear (Ref 26, 28, 29). Therefore, a pin-on-disk test against 100Cr6 steel has been stopped when the first onset of friction decrease and rapid oxidation was detected; the wear rate recorded in the standard 250 m long test is thus compared with the one measured after this shorter test and to the one measured after the 1000 m long one. While the wear rate after a 250 m sliding distance (where both adhesive and tribo-oxidative wear occur) is 19.0×10^{-5} mm^3/(Nm), the one measured in the stopped test (where only adhesive wear has occurred) is 125×10^{-5} mm^3/(Nm), one order of magnitude higher, as expected. The wear rate measured after 1000 m

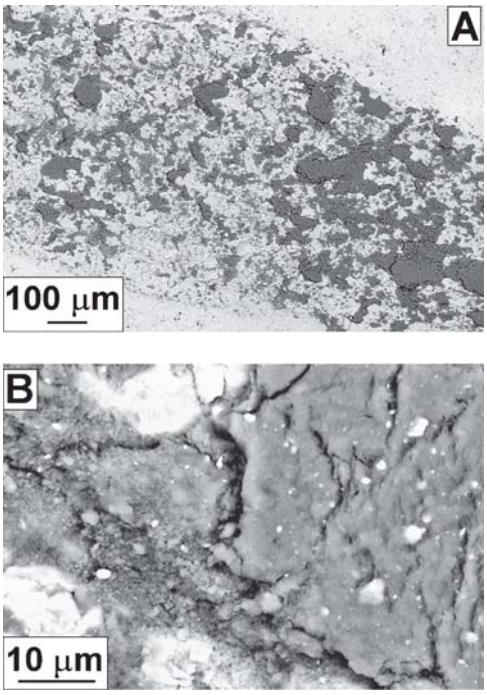

Fig. 10 SEM micrograph of as-sprayed coating wear scar after pin-on-disk test against 100Cr6 steel over a 1000 m sliding distance: (a) general view and (b) detail of oxidized areas

is 5.2×10^{-5} mm^3/(Nm); since the wear mechanisms periodically turn from adhesive to tribo-oxidative and larger portions of the wear surface are progressively covered with oxides, the overall wear rate progressively decreases.

A further test has been performed to verify that frictional heating of the coating asperities in the contact point is actually the cause of fast oxidation. The radius between the pin position and the sample rotation axis was increased from the standard 5 to 9 mm, keeping relative sliding speed constant; in this way, the pin passes less frequently over each point on the sample surface (sample revolution speed is decreased to keep sliding speed constant). The coating surface thus better dissipates heat, and its bulk temperature will increase more slowly. A lower bulk temperature means that the flash temperature of the asperities is also lower (Ref 27-30). The friction coefficient (Fig. 11) soon reaches the critical value (~0.9), but it takes a longer sliding distance to start fast oxidation and rapid friction decrease.

The different behavior observed with alumina as counterpart must now be explained. The wear scar against alumina bears evidence of abrasive wear: grooves due to plowing and/or cutting wear are noticeable (Fig. 12). Lower chemical affinity between the metallic coating and the ceramic pin reduces adhesive wear (Ref 26, 28, 29), while abrasive wear is favored by the high hardness of alumina. Nonetheless, optical micrographs show transferred coating material partly covering the alumina pin surface (Fig. 13). This suggests that some adhesion is still taking place. Besides, it is very likely that the very small wear debris produced by the abrasive processes, consisting in ductile metallic particles, can stick onto the pin surface, contributing to the rapid formation of the transfer film. Its formation promotes friction increase up to the critical oxidation temperature. Moreover,

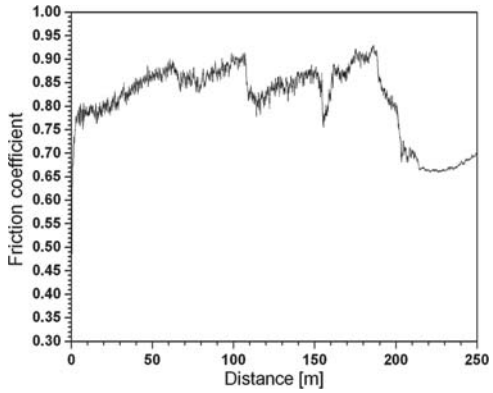

Fig. 11 Friction coefficient for the as-sprayed coating tested against 100Cr6 steel pin over a 250 m sliding distance with pin positioned 9 mm away from sample revolution axis

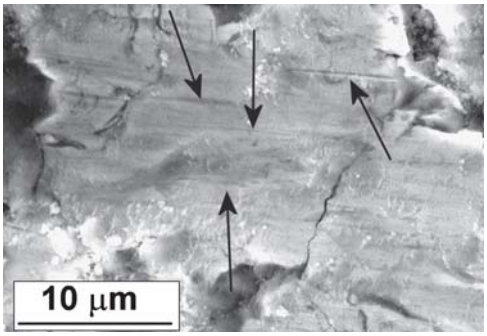

Fig. 12 SEM micrograph of as-sprayed coating tested against sintered alumina pin. Arrows indicate some abrasion grooves.

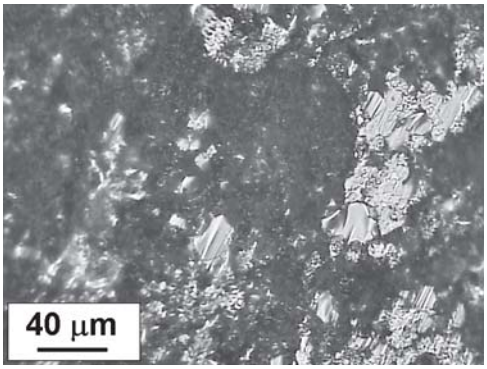

Fig. 13 Optical micrograph of sintered alumina pin after pin-on-disk test against as-sprayed coating

the much lower thermal conductivity of alumina favors higher flash temperatures on the contacting asperities than in the case of the steel pin. Indeed, formulas such as Eq 1 can be found in literature for flash temperature estimation (Ref 29):

$$T_f - T_s = 8.8 \times 10^{-4} \frac{\mu}{\sqrt{1 + 12\mu^2}} \frac{v}{k_1 + k_2} \quad \text{(Eq 1)}$$

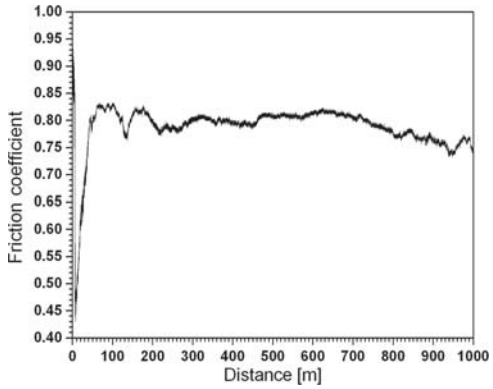

Fig. 14 Friction coefficient for the as-sprayed coating tested against sintered alumina pin over a 1000 m sliding distance

where T_s is the average surface temperature, T_f is the flash temperature, μ is the friction coefficient, and k_1, k_2 are thermal conductivities of the contacting materials.

The rapid material transfer and the high flash temperature are the reasons why friction increases faster than in the case of steel pin and why fast oxidation starts sooner.

After the fast oxidation process, the friction coefficient increases again, but, in this case, it attains a constant value, which remains constant after 250 m (Fig. 6) and also after 1000 m (Fig. 14). Scanning electron micrographs (Fig. 15) indicate that oxidized areas on the coating wear scar are finer and more numerous when compared to the coarser ones produced by the steel pin (Fig. 10A). Probably, since adhesive wear is lower in this case, the oxides formed in the rapid oxidation stage are enough to prevent repeated periodic friction increase.

The coating wear rate is lower when alumina counterparts are used: the coating heavily suffered from adhesive wear against 100Cr6 steel, but in this case (as observed previously) adhesive wear is reduced and abrasive wear is also taking place. Abrasive wear on ductile materials shows up in the form of plastic grooving, which may take place by microplowing or microcutting. The latter phenomenon consists of the formation and detachment of a chip from the surface; thus, it is definitely the most dangerous. The prevalence of microcutting or microplowing on a metallic surface depends on the geometry of the counterbody asperities and on the ductility of the metallic surface itself; a ductile surface will favor a less dangerous microplowing mechanism (Ref 26, 28, 29). The presently considered Co alloy clearly has enough ductility to prevent extensive microcutting. Thus, the wear rate is not too high; it is one order of magnitude lower that that against 100Cr6 steel.

It must be noted that the pin wear rate after 1000 m sliding distance is 1.04×10^{-5} mm^3/(Nm), substantially analogous to the 1.96×10^{-5} mm^3/(Nm) recorded after 250 m; this is consistent with the friction coefficient having reached a steady-state value.

After the 200 °C heat treatment, friction behavior is similar, but wear rates are higher; probably, the lower mechanical strength of this coating favors heavier adhesive and abrasive wear phenomena.

The 600 °C heat treated sample wear loss against steel pin is negligible, and the steel pin wear rate is almost two orders of magnitude lower (Table 1). The friction coefficient has no

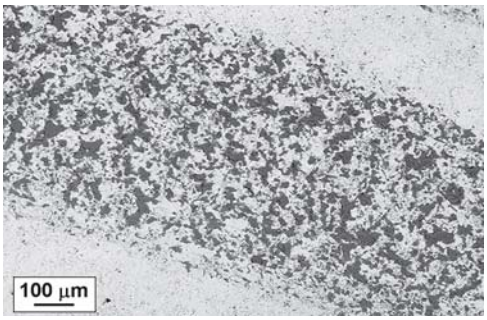

Fig. 15 SEM micrograph of as-sprayed coating wear scar after pin-on-disk test against sintered alumina pin over a 1000 m sliding distance

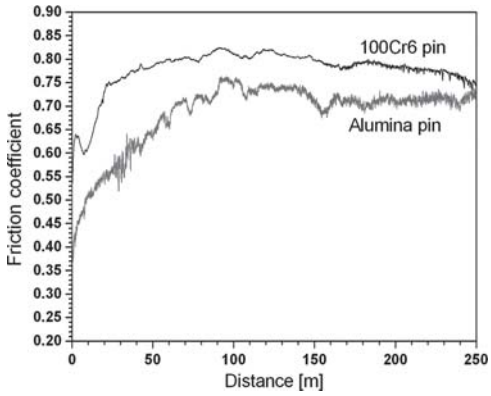

Fig. 16 Friction coefficient for the 600 °C heat treated coating tested against 100Cr6 steel and sintered alumina pins over a 250 m sliding distance

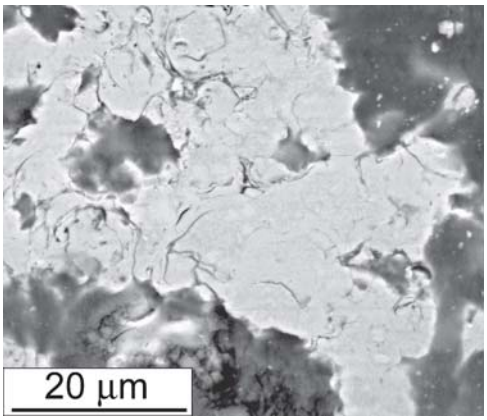

Fig. 17 SEM micrograph of 600 °C heat treated coating after pin-on-disk test against 100Cr6 steel pin

peaks, but attains a steady value, slightly lower than the final value of former coatings (Fig. 16), and no fast oxidation is detectable. The friction coefficient stability is also retained after a 1000 m sliding distance. The increased coating microhardness now largely prevents adhesion, as confirmed by SEM micrographs (Fig. 17) showing the original polished surface of the sample is unaltered. This explains both the decrease in coating and pin

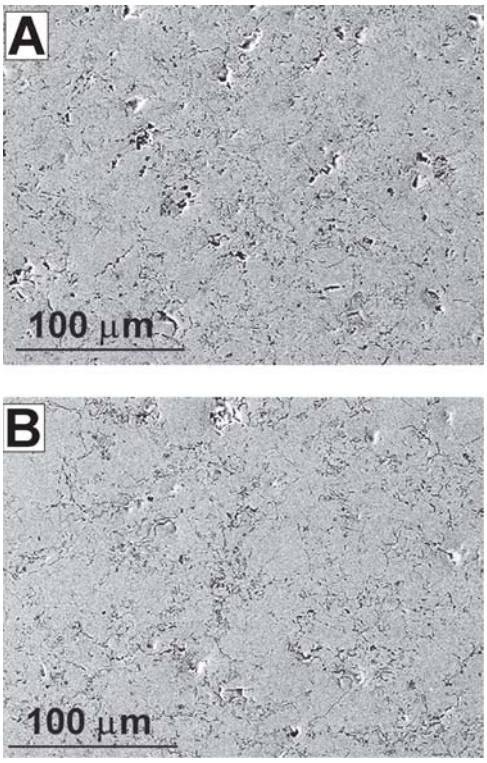

Fig. 18 SEM micrographs of polished surfaces of (a) as-sprayed and (b) 600 °C heat treated coatings

wear rates and the disappearance of peaks in the friction coefficient evolution. Some wear scar oxidation still occurs, but fast oxidation with much wear debris was never detected.

In the test against alumina, the sample and pin wear rates resemble those for as-sprayed and 200 °C heat treated coatings, and abrasive wear seems to be once again the prevailing wear mechanism. The higher mechanical strength of the 600 °C heat treated coating might have had two different outcomes in pin-on-disk tests against alumina. On the one hand, higher coating hardness could have lowered grooving phenomena, thus reducing the wear rate; on the other, higher hardness might have resulted in lower ductility, promoting microcutting phenomena and increasing the wear rate. Apparently, none of these phenomena actually occurred. The hardness difference between alumina pin and metallic coating is still very high; thus, abrasive grooving cannot be significantly lessened. At the same time, the coating material has preserved enough plasticity to prevent extensive cutting, as in the as-sprayed condition. Nonetheless, further reduction of adhesion between coating and pin accounts for the disappearance of fast oxidation and friction coefficient peaks in the test against alumina (Fig. 6); so, some advantageous effects of the 600 °C heat treatment also emerge with alumina counterbody.

There might be a second hypothesis for the friction coefficient stability of the 600 °C heat treated sample both against steel and against alumina: the heat treatment may have formed a significant amount of self-lubricating oxides inside the coating. However, SEM micrographs of the polished surfaces of the as-sprayed and 600 °C heat treated coatings (Fig. 18a and b) both show a similar degree of oxide inclusions, due to splat boundary oxide stringers produced during coating deposition, as discussed previously. Energy dispersive spectroscopy analyses have also been performed on three different regions for both polished surfaces: chemical analysis by energy dispersive x-ray spectrometry can only be regarded as semiquantitative due to the measurement uncertainties, but the O wt.%/Co wt.%, Cr wt.%/Co wt.%, Mo wt.%/Co wt.%, Si wt.%/Co wt.% ratios can be compared for the as-sprayed and 600 °C heat treated coatings (Table 2). The values are substantially similar, thus indicating that there is no significant chemical composition difference between the as-sprayed and 600 °C heat treated coatings.

Therefore, it can be concluded that the microstructural modification induced by the heat treatment is mainly responsible for the improvement in coating performance.

4. Conclusions

The current study examined the tribological behavior of HVOF sprayed Co-28%Mo-17%Cr-3%Si coatings, both as-deposited and after heat treatments, correlating it with microstructural and micromechanical features. A significant degree of splat boundary oxidation exists in the as-sprayed coating, because of exothermic oxidative reaction occurring at $T > 810$ °C. This coating is mainly amorphous due to splat quenching; thus, it has low hardness and toughness, resulting in poor tribological performance—particularly, its low hardness promotes adhesive wear against 100Cr6 steel pins. Adhesion causes a rapid increase in friction coefficient, and consequently the contact point temperature reaches a critical value where rapid oxidation occurs. Oxides decrease the friction coefficient, but they are not particularly adherent to the contacting surfaces and mostly form debris. Therefore, friction increases again and continues to oscillate periodically because adhesive wear continues to raise flash temperature up to the critical value. Most of the wear loss occurs in the first stage, where adhesion is particularly severe due to direct contact between metallic surfaces. In the tests against alumina pin, the sample wear rate is smaller because less adhesion takes place; abrasive wear is prevalent, but the Co-base alloy has sufficient intrinsic plasticity to withstand it without undergoing too much cutting wear. However, the fast oxidation process, with peculiar friction coefficient behavior, still takes place.

While the 200 and 400 °C heat treatments do not cause any major change (the former one even degrading the coating properties), the 600 °C treatment causes the appearance of submicrometric crystalline regions improving hardness and elastic modulus. Adhesive phenomena between coating and steel pin are thus definitely reduced; the wear loss is negligible for the coating and decreased by two orders of magnitude for the pin; no friction coefficient peaks occur nor is fast oxidation started. Instead, friction coefficient soon gets to a steady value. The coating wear rate against alumina pin is not significantly changed because abrasive wear still prevails, so there are no major changes in the wear process. However, adhesive phenomena are further reduced, preventing the appearance of friction coefficient peaks and of fast oxidation. Thus, performing a 600 °C, 1 h heat treatment in air could be suggested as a way to improve the sliding wear performance of the present alloy at room temperature. The 600 °C heat treated coating wear rates are lower than those recorded by the authors for hard chrome platings at room temperature under the same testing conditions (Ref 31).

Table 2 Chemical composition of the polished surface of as-sprayed and 600 °C heat treated coatings, from EDS analysis

	(O wt.%/Co wt%) × 100	(Cr wt.%/Co wt.%) × 100	(Mo wt.%/Co wt.%) × 100	(Si wt.%/Co wt.%) × 100
As-sprayed	6.48 ± 1.75	36.56 ± 0.27	58.47 ± 0.23	6.30 ± 0.24
600 °C heat treated	5.80 ± 0.38	37.54 ± 0.08	58.30 ± 1.00	7.09 ± 0.58

Note: Data are expressed as percent ratios between weight percentages of the various elements and the weight percentage of Co (the main constituent).

Acknowledgments

Many thanks to ing. Sara Riccò for her contribution to experimental characterization and to Prof. Federica Bondioli for DTA-TG analysis. The authors gratefully acknowledge ing. Fabrizio Casadei, Mr. Edoardo Severini, and Mr. Francesco Barulli, Centro Sviluppo Materiali S.p.A. (Roma, Italy) for coatings manufacturing. Partially supported by PRRIITT (Regione Emilia Romagna), Net-Lab "Surface & Coatings for Advanced Mechanics and Nanomechanics" (SUP&RMAN).

References

1. M.R. Dorfman, Thermal Spray Materials, *Adv. Mater. Process.,* 2002, **160**(9), p 49-51
2. E. Turunen, T. Varis, T.E. Gustafsson, J. Keskinen, T. Fält, and S.-P. Hannula, Parameter Optimization of HVOF Sprayed Nanostructured Alumina and Alumina-Nickel Composite Coatings, *Surf. Coat. Technol.,* 2006, **200,** p 4987-4994
3. H.M. Hawthorne, B. Arsenault, J.P. Immarigeon, J.G. Legoux, and V.R. Parameswaran, Comparison of Slurry and Dry Erosion Behavior of Some HVOF Thermal Sprayed Coatings, *Wear,* 1999, **225-229**(2), p 825-834
4. J. Barber, B.G. Mellor, and R.J.K. Wood, The Development of Subsurface Damage During High Energy Solid Particle Erosion of a Thermally Sprayed WC-Co-Cr Coating, *Wear,* 2005, **259**(1), p 125-134
5. P.L. Ko and M.F. Robertson, Wear Characteristics of Electrolytic Hard Chrome and Thermal Sprayed WC-10 Co-4 Cr Coatings Sliding Against Al-Ni-bronze in Air at 21 °C and at −40 °C, *Wear,* 2002, **252**(11-12), p 880-893
6. T. Sahraoui, N.-E. Fenineche, G. Montavon, and C. Coddet, Alternative to Chromium: Characteristics and Wear Behavior of HVOF Coatings for Gas Turbine Shafts Repair (Heavy-Duty), *J. Mater. Process. Technol.,* 2004, **152**(1), p 43-55
7. F. Rastegar and D.E. Richardson, Alternative to Chrome: HVOF Cermet Coatings for High Horsepower Diesel Engines, *Surf. Coat. Technol.,* 1997, **90**(1-2), p 156-163
8. S. Stewart, R. Ahmed, and M.T. Itsukaichi, Rolling Contact Fatigue of Post-Treated WC–NiCrBSi Thermal Spray Coatings, *Surf. Coat. Technol.,* 2005, **190**(2-3), p 171-189
9. M.P. Planche, H. Liao, and C. Coddet, Comparison of In-Flight Particle Characteristics and Coating Properties While Spraying NiCrBSi Powder with Different Spraying Processes, *Thermal Spray 2004: Advances in Technology and Application,* May 10-12, 2004 (Osaka, Japan), ASM International, 2004, p 235-239
10. H.M. Hawthorne, B. Arsenault, J.P. Immarigeon, J.G. Legoux, and V.R. Parameswaran, Comparison of Slurry and Dry Erosion Behaviour of Some HVOF Thermal Sprayed Coatings, *Wear,* 1999, **225-229,** p 825-834
11. M.A. Uusitalo, P.M.J. Vuoristo, and T.A. Mäntylä, Elevated Temperature Erosion-Corrosion of Thermal Sprayed Coatings in Chlorine Containing Environments, *Wear,* 2002, **252,** p 586-594
12. D.W. Wheeler and R.J.K. Wood, Erosion of Hard Surface Coatings for Use in Offshore Gate Valves, *Wear,* 2005, **258**(1-4), p 526-536
13. M.K. Stanford and V.K. Jain, Friction and Wear Characteristics of Hard Coatings, *Wear,* 2001, **251,** p 990-996
14. L. Gil, M.A. Prato, and M.H. Staia, Effect of Post-Heat Treatment on the Corrosion Resistance of NiWCrBSi HVOF Coatings in Chloride Solution, *J. Therm. Spray Technol.,* 2002, **11**(1), p 95-99
15. T. Sahraoui, H.I. Feraoun, N. Fenineche, G. Montavon, H. Aourag, and C. Coddet, HVOF-Sprayed Tribaloy-400: Microstructure and First Principle Calculations, *Mater. Lett.,* 2004, **58**(19), p 2433-2436
16. G. Xiao-Xi and H. Zhang, HVOF-Sprayed Tribaloy (T-800): Microstructure and Particle-Erosion Behaviour, *Thermal Spray: International Advances in Coatings Technology*, May 25 to June 5, 1992 (Orlando, FL), C.C. Berndt, Ed., ASM International, 1992, p 729-734
17. G. Bolelli, V. Cannillo, L. Lusvarghi, and S. Riccò, Mechanical and Tribological Properties of Electrolytic Hard Chrome and HVOF-Sprayed Coatings, *Surf. Coat. Technol.,* 2006, **200,** p 2995-3009
18. D.C. Crawmer, J.D. Krebsbach, and W.L. Riggs, Coating Development for HVOF Process Using Design of Experiment, *Thermal Spray: International Advances in Coatings Technology*, May 25 to June 5, 1992 (Orlando, FL), C.C. Berndt, Ed., ASM International, 1992, p 127-136
19. "Validation of WC-Co, WC-Co-Cr HVOF or Tribaloy 800 Thermal Spray Coatings as a Replacement for Hard Chrome Plating on C-2/E-2/P-3 and C-130 Propeller Hubs and Low Pitch Stop Lever Sleeve," U.S. Hard Chrome Alternatives Team (HCAT), Joint Group on Pollution Prevention (JG-PP), and Canadian Hard Chrome Alternatives Team (C-HCAT), Joint Test Protocol, Nov 17, 1999, available upon request
20. T. Sahraoui, S. Guessasma, N.E. Fenineche, G. Montavon, and C. Coddet, Friction and Wear Behaviour Prediction of HVOF Coatings and Electroplated Hard Chromium Using Neural Computation, *Mater. Lett.,* 2004, **58**(5), p 654-660
21. H. Koiprasert, S. Dumrongrattana, and P. Niranatlumpong, Thermally Sprayed Coatings for Protection of Fretting Wear in Land-Based Gas-Turbine Engine, *Wear,* 2004, **257**(1-2), p 1-7
22. H. Choi, S. Yoon, G. Kim, H. Jo, and C. Lee, Phase Evolutions of Bulk Amorphous NiTiZrSiSn Feedstock During Thermal and Kinetic Spraying Processes, *Scr. Mater.,* 2005, **53**(1), p 125-130
23. W.C. Oliver and G.M. Pharr, An Improved Technique for Determining Hardness and Elastic Modulus using Load and Displacement Sensing Indentation Experiments, *J. Mater. Res.,* 1992, **7,** p 1564-1583
24. A.G. Evans and E.A. Charles, Fracture Toughness Determinations by Indentation, *J. Am. Ceram. Soc.,* 1976, **59**(7-8), p 371-372
25. C. Verdon, A. Karimi, and J.-L. Martin, A Study of High Velocity Oxy-fuel Thermally Sprayed Tungsten Carbide Based Coatings. Part 1: Microstructures, *Mater. Sci. Eng., A-Struct.,* 1998, **246**(1-2), p 11-24
26. B. Bhushan, Wear, *Principles and Applications of Tribology,* 1st ed., J. Wiley & Sons, New York, 1999, p 479-585
27. B. Bhushan, Interface Temperature of Sliding Surfaces, *Principles and Applications of Tribology,* 1st ed., J. Wiley & Sons, New York, 1999, p 431-478
28. K. Kato and K. Adachi, Wear Mechanisms, *Modern Tribology Handbook,* Vol 1*,* 1st ed., B. Bhushan Ed., CRC Press, 2001, p313-315
29. G. Straffelini, *Attrito e usura—Metodologie di progettazione e controllo,* Tecniche Nuove, Milano, Italy, 2005, in Italian
30. M.F. Ashby, J. Abulawi, and H.S. Kong, Temperature Maps for Frictional Heating in Dry Sliding, *Tribol. T.,* 1991, **34**(4), p 577-587
31. G. Bolelli, V. Cannillo, L. Lusvarghi, and T. Manfredini, Wear Behaviour of Thermally Sprayed Ceramic Oxide Coatings, *Wear,* in press